Corrosion propagation monitoring using electrochemical noise measurements on carbon steel in hydrogenocarbonated solution containing chloride ions

Chloé Comas, François Huet, Kieu Ngo, Marion Fregonese, Hassane Idrissi, Bernard Normand

Corrosion propagation monitoring using electrochemical noise measurements on carbon steel in hydrogenocarbonated solution containing chloride ions

Chloé Comas, François Huet, Kieu Ngo, Marion Fregonese, Hassane Idrissi, Bernard Normand

PII: S0010-938X(21)00651-X

DOI: https://doi.org/10.1016/j.corsci.2021.109885

Reference: CS109885

To appear in: *Corrosion Science*

Received date: 30 June 2021
Revised date: 4 October 2021
Accepted date: 11 October 2021

Please cite this article as: Chloé Comas, François Huet, Kieu Ngo, Marion Fregonese, Hassane Idrissi and Bernard Normand, Corrosion propagation monitoring using electrochemical noise measurements on carbon steel in hydrogenocarbonated solution containing chloride ions, *Corrosion Science,* (2021) doi:https://doi.org/10.1016/j.corsci.2021.109885

Corrosion propagation monitoring using electrochemical noise measurements on carbon steel in hydrogenocarbonated solution containing chloride ions

Chloé Comas[a,*], François Huet[b], Kieu Ngo[b], Marion Fregonese[a], Hassane Idrissi[a], Bernard Normand[a]

[a] Université de Lyon, INSA Lyon, MATEIS, UMR CNRS 5510, F-69621 Villeurbanne, France

[b] Sorbonne Université, CNRS, Laboratoire Interfaces et Systèmes Electrochimiques, F-75005 Paris, France

ABSTRACT

The propagation of localized corrosion on API 5L X65 carbon steel in hydrogenocarbonated solution containing chloride ions was monitored during long immersion times by electrochemical noise (EN) measurements in ZRA mode. Monitoring corrosion propagation from the EN amplitude is possible but interpreting the potential and current transients after long immersion times is made difficult by the different corrosion processes (metastable or stable pits, crevices, corrosion products detachment…) occurring simultaneously. The noise impedance at 0.1 Hz, directly derived from the EN measurements, is shown to decrease and stabilize in the same time scale as the coupled potential of the electrodes.

Keywords: localized corrosion, carbon steel, open circuit potential, electrochemical noise measurements, noise impedance

* Corresponding author.

E-mail address: chloe.comas@insa-lyon.fr (C. Comas)

1. Introduction

Localized corrosion sometimes occurs freely on passive surfaces in the presence of aggressive anionic species like chloride ions. It proceeds according to several stages: passive film breakdown and metastable pitting, then stable pit growth. When localized corrosion occurs, an electrochemical coupling is established between the free surfaces and the confined zones in which the chemical composition of the medium is strongly modified [1,2]. Many authors studied localized corrosion of carbon steel at Open Circuit Potential (OCP) or under polarization in different passivating media containing chloride ions such as simulated concrete pore solution [3,4], saturated $Ca(OH)_2$ [3,5–7], $NaNO_2$ [8,9], or $NaHCO_3$ [8,10–11] using deterministic electrochemical techniques (polarization curves, electrochemical impedance spectroscopy (EIS)…).

Localized corrosion of carbon steel induced by chloride ions in these environments was also studied by Electrochemical Noise Measurements (ENM) to detect the onset of corrosion, identify its mechanism and quantify the damage caused by a given corrosion mode [6,12–14]. It is well known that ENM presents potentialities for such application [15,16]. This non-intrusive technique consists in measuring the random fluctuations of electrical parameters such as the potential of the electrode and/or the current flowing through it when an electrochemical process takes place at the material-environment interface. Measurements can be carried out in galvanostatic, potentiostatic or zero resistance ammeter (ZRA) modes. The latter mode involves two electrodes, most commonly identical, coupled to each other to measure both current and voltage fluctuations. The current generated by the electrochemical processes is measured between the two electrodes while their coupling potential is monitored using a reference electrode [17,18]. A metastable corrosion process (breakdown and repassivation of passive film) can often be identified from the signature of the current or potential transients that can have different shapes according to the metal undergoing corrosion: for stainless steel, the current transient due to a pit is characterized by a slow rise followed by a sharp drop while a sudden rise followed by a slow decay can be observed for carbon

steel [15]. Potential transients can present such characteristics too but they are also influenced by the charge and discharge of the capacitance of the passive film [12].

The objective of the present paper is to investigate propagation of localized corrosion on API 5L X65 carbon steel during long immersion times (up to 100 hours) in $NaHCO_3$ aqueous solution containing chloride ions at OCP using ENM and to evaluate the capacities and limitations of the EN technique for such study. Indeed, the EN technique is generally used to detect the onset of localized corrosion, not its propagation on long times. Great care was taken for validating the ENM and identify the influence of the instrumentation noise sometimes present.

2. Experimental

The tested material was an API 5L X65 grade carbon steel whose chemical composition is given in Table . The samples were rectangular plates of 30 x 100 mm dimensions and thickness of 3 mm (Fig. 1). After grinding up to 1200 grit SiC paper, one side and the cut edges of the samples were covered with a thin layer of cataphoretic paint (black colour in Fig. 1) commonly used in the automotive industry for its anticorrosion properties, leaving one side of 7.5 or 1.5 cm^2 surface area exposed to solution.

The solution used for studying the propagation of localized corrosion was 0.5 M $NaHCO_3$ + 0.2 M NaCl (pH 8-9), a chloride concentration high enough to develop localized corrosion sites on a short time delay at OCP [8,10–13]. The samples were first–immersed in the chloride-free 0.5 M $NaHCO_3$ solution during 15 min to form a protective film barrier before being immersed in the testing solution at room temperature.

The experimental cell was composed of a saturated calomel electrode (SCE) as reference electrode and two identical carbon steel samples, held vertically at a distance of 8 mm, as working electrodes in a beaker containing approximately 2 L of solution, which was opened to air. OCP monitoring, EIS and EN measurements were performed using a Gamry® REF 600^+

potentiostat/galvanostat. As soon immersed in the solution, the electrodes were coupled in ZRA mode. Besides the coupling potential, the OCP of each electrode was also measured when the electrical circuit was opened before performing EIS measurements. Impedance spectra were measured on each electrode polarized at the coupling potential in the frequency range from 100 kHz to 0.1 or 0.01 Hz, using an AC voltage amplitude of 10 mV_{rms}.

After each test, the corrosion products were removed from the samples according to ASTM standard G1-03(2017) E1 and the morphology of the electrode surface was observed with a scanning electron microscope (SEM).

3. Electrochemical noise measurements

3.1. Procedure and validation

ENM were performed using the Gamry® ESA 410® software in ZRA mode. The electrochemical cell was placed in a Faraday cage connected to the floating ground of the potentiostat in order to reduce the mains interference (50 Hz and harmonics) [19]. In this work, the noise measurements were performed in three successive steps by using sampling frequencies f_s of 10 Hz during 28 min, 1 Hz during 70 min and 10 Hz during 28 min with an I-E range of 6 or 60 µA corresponding to a current-measuring resistance of 20 kΩ or 2 kΩ, respectively [20]. Using two different sampling frequencies allows a first validation of the ENM by checking that the power spectral densities (PSDs) overlap well in the common frequency ranges. A good overlap can only be obtained if anti-aliasing filters are present before the analog-to-digital converters in the voltage and current measuring channels of the potentiostat, which is not the case in many commercial equipment [21]. In this work, the three-step procedure was used to check the stationarity of the signals from the overlap quality of the PSDs. Indeed, a PSD can only be defined for stationary signals, that is, signals whose statistical properties do not evolve in time.

Data processing in the frequency domain was carried out with the European Cooperative Group on Corrosion Monitoring of Nuclear Materials (ECG-COMON) software (available for free on www.ecg-comon.org [22]). The PSDs were calculated by dividing each raw data ASCII file in 8 sections of N (2,048 for f_s = 10 Hz or 512 for f_s = 1 Hz) data points to get averaged PSDs in the frequency bandwidth [f_s/N, $f_s/2$] by using the fast Fourier transform (FFT) after having linearly detrended each section and applied Hann window on the detrended section [19,20].

Preliminary ENM in ZRA mode were carried out to determine the noise of the instrumentation with dummy cells composed of three identical resistors R in a star arrangement (R = 100 Ω to10 kΩ) in an attempt to measure the thermal noise generated by the resistors. An I-E range of 6 and 60 µA and two sampling frequencies (10 Hz and 1 Hz) were used, as for the corroding system. The evaluation of the instrumental noise prior to ENM in corrosion studies is essential to (i) validate the ability of the instrument to perform reliable measurements on a simple stationary system, (ii) quantify this noise for assessing its influence on subsequent ENM on complex systems, and (iii) determine the frequency domain in which the corrosion processes produce a noise greater than the instrumentation noise.

It has been shown that the PSDs of the voltage and current thermal noise generated by a dummy cell in ZRA mode are equal to $6kTR$ and $2kT/R$, respectively, where k represents the Boltzmann constant, T the temperature in Kelvin and R the dummy cell resistance [21]. Unfortunately, for R values lower than 1 MΩ, the potential and current thermal noise cannot be measured because the instrumentation noise is much higher. This has been experimentally checked for R values ranging between 10 Ω and 100 kΩ. To go further, the noise sources of the potentiostat used have been identified so that the PSDs of the measured signals could be calculated for two working electrodes (WE) of impedance Z_1 and Z_2 connected in ZRA mode [20]:

$$\Psi_{E_{meas}} = \left|\frac{Z_1 Z_2}{Z_1+Z_2}\right|^2 \left(\Psi_{i_1} + \Psi_{i_2}\right) + \Psi_{e_{Ref}} + \Psi_{e_{n,v}} + \left|\frac{Z_1}{Z_1+Z_2}\right|^2 \Psi_{e_n} \quad (1)$$

$$\Psi_{I_{meas}} = \frac{|Z_1|^2\,\Psi_{i_1} + |Z_2|^2\,\Psi_{i_2}}{|Z_1+Z_2|^2} + \frac{\Psi_{e_n}}{|Z_1+Z_2|^2} + \frac{\Psi_{e_{n,i}}}{R_m^2} + \frac{4kT}{R_m} \quad (2)$$

where R_m is the current-measuring resistance, i_1, i_2 are the noise sources due to the corrosion processes, e_{Ref} the voltage noise of the reference electrode (RE), $e_{n,v}$ the voltage noise of the potential amplifier, $e_{n,i}$ the voltage noise of the current amplifier, and e_n the sum of the voltage noise of the other amplifiers of the potentiostat. Here, Eqs. 1 and 2 have been simplified for the case of low R_m values (2 and 20 kΩ) used in this work [20].

In the case of dummy cells with three identical resistors, Eqs. 1 and 2 are reduced to [20]:

$$\Psi_{E_{meas}} = 6kTR + \Psi_{e_{n,v}} + \frac{1}{4}\Psi_{e_n} \quad (3)$$

$$\Psi_{I_{meas}} = \frac{2kT}{R} + \frac{1}{4R^2}\Psi_{e_n} + \frac{\Psi_{e_{n,i}}}{R_m^2} + \frac{4kT}{R_m} \quad (4)$$

The last two terms in Eq. 3 and three last terms in Eq. 4 correspond to the voltage noise and current noise of the instrumentation.

3.2. Characterization of the instrumentation noise

The instrumentation noise of the potentiostat Gamry REF 600$^+$ was determined using dummy cells of various resistances *R*. Fig. 2 shows the PSDs of the potential noise and current noise measured with each dummy cell at sampling rates of 1 Hz and 10 Hz. The PSD overlaps in the common frequency ranges are perfect for each dummy cell and each I-E range thanks to the presence of anti-aliasing filters before the analog-to-digital converters in the potential and current measurement channels. The effect of the filters is shown by the strong decrease of the PSDs at frequencies slightly less than $f_s/2$.

The results confirm that the Gamry REF 600$^+$ potentiostat used in this work is able to perform reliable EN measurements. The level of the potential PSDs in Fig. 2a is much higher than that of the potential thermal noise generated by the dummy cell (for example, $6kTR = 2.4 \times 10^{-16}$

V^2/Hz for R = 10 kΩ), which indicates that the potential noise was generated by the potentiostat itself. The analysis of the current PSDs in Fig. 2b is more involved since they depend on both the dummy cell resistance R and current-measuring resistance R_m, as expected from Eq. 4. In all cases, the measured current noise was due to the instrumentation since the PSD level is much higher than that of the current thermal noise (for example, $2kT/R = 0.8 \times 10^{-22}$ A^2/Hz for R = 100 Ω). Once determined, the PSDs of the instrumentation noise will be compared below to those of the EN measured on the corrosion systems.

4. Results and discussion

4.1. Preliminary study

Fig 3a. presents the time evolution of the OCP of single API 5L X65 carbon steel electrodes of surface area of 27.3 cm^2 immersed in 0.5 M $NaHCO_3$ without, for test 1, or with 0.2 M NaCl for the three other tests. In 0.5 M $NaHCO_3$, the free corrosion potential of the electrode shifted to positive values resulting from the formation of a protective barrier layer on the metal [10,23]. Indeed, $NaHCO_3$ reacts with ferric ions when the concentration of HCO_3^- is high enough to saturate the solution and stabilize the $FeCO_3$ concentration [4,9–11].

After pre-immersion for 15 min in 0.5 M $NaHCO_3$, the corrosion potential of the sample was approximately -240 mV / SCE. Then, after immersion in 0.5 M $NaHCO_3$ + 0.2 M NaCl (Fig. 3a), the corrosion potential, initially around −250 mV vs. SCE, decreased during the first 20 to 60 hours of immersion and stabilized around −425 mV vs. SCE. This decrease in potential reflects a change in the electrochemical behavior and in the nature of the layer present on the steel surface, following the activation of the material due to the addition of chloride ions. The same behavior was observed during tests 5 to 7 in which the two electrodes were continuously coupled through the ZRA, except in test 6 where the electrical circuit was opened from time to time to measure the free potential and the impedance of each electrode (Fig. 3b): the coupled potential of the electrodes decreased and

stabilized in the same time and potential scales. These results indicate that the electrodes were macroscopically comparable during tests 1 to 7 and underwent the same overall surface evolution, regardless of the electrode size or the type of connection, single or coupled samples. The similar OCP evolution — time trend and numerical values — of the individual and coupled electrodes is an evidence of the robustness and reliability not only of the OCP measurements but also the interface control through the ZRA, which is expected to apply a zero-volt potential difference between the two electrodes while allowing them to freely evolve as if they were in actual isolated but connected conditions.

In view of the large amplitude of the potential fluctuations observed in Fig. 3, localized corrosion attacks of the material can be expected, which corresponds well to the usual effect of chlorides on a pseudo-passivated material. Indeed, at the free corrosion potential, the formed layer is not sufficiently stable to maintain the protection of the steel over the entire surface and localized corrosion can develop. Later, the corrosion potential of the sample stops decreasing when the layer formation/dissolution counteracting effects reached steady-state conditions (Fig. 3).

Fig. 4 shows SEM images of the surface of a sample after 115 hours of immersion and removal of the corrosion products. The surface is covered by pits of micrometer size like the one presented in Fig. 4a, but it also exhibits larger corrosion attacks, of millimeter size like the one shown in Fig. 4b. These attacks are formed by general dissolution areas and micrometer pits with smaller pits distributed inside and around as presented in Fig. 4c.

The local breakdown of the barrier layer is due to the adsorption of chloride ions that leads to the nucleation of pits. Some pits are metastable and stop growing, others are stable and can propagate, all of them being the source of corrosion products. New metastable pits then develop under the corrosion products by propagation of the active areas in the stable pits already formed. Indeed, the growth of the stable pits produces Fe^{2+} ions that attract chloride ions inside the pit cavity and enhance the pit growth and, furthermore, lead to the formation of porous corrosion products

above the pits, by reaction with hydroxide and bicarbonate ions from the bulk solution. The anion-selective nature of the rust layer and its local enrichment in chloride ions then favors the development of new metastable pits under the deposit of corrosion products. New metastable pits can also develop around the corrosion products by crevice-inducing pit initiation [6]. According to these authors, this is linked to the expansion of the surface area of the rust cover above the pit cavity, possibly forming an annular micro-crevice on the steel along the external boundary of the corrosion deposit. Competition between the hydroxide and chloride ions in the micro-crevice leads to the repeated nucleation and repassivation of metastable pits in the active areas covered by the corrosion products. Then, the confinement in the pit cavities by corrosion products induced the local acidification of the active areas and then lead to the coalescence of the stable and metastable pits, the propagation of the stable pits contributing to the growth of the millimeter corrosion attacks areas in both horizontal and perpendicular directions.

4.2. ENM performed on 7.5 cm² electrodes during test 5

In test 5, the two identical API 5L X65 electrodes of surface area 7.5 cm^2 were immersed in the solution for a hundred hours. The electrical circuit was never opened to perform EIS or OCP measurements so that the two electrodes remained connected through the ZRA during the whole test. Fig. 5 shows that only one electrode presented a millimeter corrosion attack at the end of the immersion.

Validation of EN measurements, which is an essential step to avoid errors in data interpretation, is based on the analysis of the potential and current PSDs. It is indeed impossible to validate EN measurements from the only analysis of time records that give no information on the possible aliasing of high to low frequencies and do not indicate whether the recorded noise comes from the corrosion system or from the instrumentation. As a matter of fact, the noise of the measuring equipment may be of higher level than the noise generated by the corrosion system. This happens, in particular, when the EN recording parameters are not optimized and/or when very low

noise systems, such as passive electrodes, are studied. As explained above, the influence of the instrumentation noise is assessed by comparing the potential and current PSDs of the noise measured on the corrosion system to those of the noise generated by dummy cells of impedance close to that of the system studied. When EIS measurements have not been performed, as in test 5, the impedance modulus of the corrosion system can be estimated from the noise impedance Z_n, defined as the square root of the ratio of the potential PSD to the current PSD. Indeed, when ENM are performed with two identical electrodes and a true reference electrode in a conductive solution, it has been shown that Z_n is equal to the impedance modulus of the electrodes when the instrumentation noise can be neglected [24].

Fig. 6 presents the current and potential PSDs together with the noise impedance measured at different immersion times. All PSDs measured at sampling rates 1 Hz and 10 Hz overlap well in the common frequency ranges, indicating that the signals are stationary during their measurement times. However, the PSD level varied with the immersion time, starting at a low level and increasing/decreasing as a function of the intensity of the corrosion attacks. Roughly speaking, below 1 Hz, the measured noise came from the corrosion processes while above 1 Hz the noise was sometimes due to the instrumentation. This is clearly shown for the potential PSDs in Fig. 6b whose levels are much higher than that of the PSD of the instrumentation noise presented in Fig. 2a, except at frequencies above 1 Hz. This is less clear for the current PSDs in Fig. 6a because the current noise depends on both the electrode impedance and I-E range (60 µA in test 5). The reasoning is the following: according to Fig. 6c, the noise impedance, which is free of instrumentation noise below 1 Hz, ranges between 0.8 and 3 kΩ at 0.1 Hz and in that case Fig. 2b shows that the amplitude of the current PSD of the instrumentation noise is lower than 3×10^{-18} A^2/Hz, which is much below the amplitude of the PSDs in Fig. 6a. However, at 1 Hz, Z_n is close to 100 Ω so that the PSD of the instrumentation noise is equal to 2×10^{-17} A^2/Hz, which is close to the PSD level of the measured current noise. It should be noticed that the reasoning is only approximate since it is based on the use

of dummy cells of constant resistance while the electrode impedances vary with frequency. It is simpler to consider that when the current PSD flattens or slightly increases with frequency above 1 Hz in Fig. 6a, this is a clear indication of the preponderance of the instrumentation noise (see Eq. 18 and Fig. 6 in [25]).

Fig. 6c shows that the noise impedance decreased with time during the first fifty hours of immersion and then stabilized. At the beginning of immersion, both electrodes had the same impedance so that the noise impedance was equal to the electrode impedance modulus, which is a well-known result for identical electrodes [24]. However, after some immersion time, only WE1 presented localized attacks, which is confirmed by the good correlation between the potential and current time records in Fig. 7. It could a priori be expected that the decrease in noise impedance with time is related to the decrease of the impedance modulus of the corroding electrode WE1. However, in that case of asymmetric systems ($|Z_1|$ would be lower than $|Z_2|$), it has been shown that Z_n measures the impedance modulus of the less noisy electrode, that is, the less corroding electrode, here WE2, thanks to the noise generated by the noisy WE1 that serves as excitation signal [26]. The decrease in Z_n, by a factor of 3.2 at 0.1 Hz from 7 to 97 hours of immersion, is then an indication that $|Z_2|$ also decreased even if WE2 showed no millimeter corrosion attack at the end of immersion. This could be due to a thinning of the protective barrier layer on WE2, which is consistent with the fact that Z_n and the coupled electrode potential clearly followed the same time evolution, according to Fig. 6d. This should be corroborated with other experiments in which EIS measurements would also be performed. This was the aim of test 6 below.

Fig. 7 presents the potential and current time records at different sampling rates and immersion times. Thanks to the previous analysis of the PSDs, it can be claimed that all fluctuations were generated by the corrosion processes, except for the current record sampled at 10 Hz in Fig. 7a where the 20 nA fast fluctuations observed around the curve were attributed to the instrumentation because the corresponding current PSD in Fig. 6a flattens above 1 Hz. Until 50 hours of immersion,

the mean current flowing in solution was low and simultaneous potential and current transients characteristic of metastable pitting corrosion can be observed in both positive and negative directions, indicating that both WEs were corroding (Fig. 7abc). Indeed, the direction of the current peaks depends on which electrode pitting occurs, while the associated potential peaks are always in the negative direction. After 50 hours of immersion, the mean current increased drastically in the negative direction (up to 30 µA in absolute value), indicating that WE1 was preferentially corroding (Fig. 7d). In that case of asymmetrical systems, the anodic reactions were enhanced on WE1, which polarized the cathodic reactions on WE2, both processes contributing to the depassivation of the WEs and, therefore, to their drop in impedance.

Current fluctuations of higher amplitude could also be observed, with a perfect correlation with the potential fluctuations, which explains why the noise impedance in Fig. 6c was so precise at long immersion times. It should be noticed that the appearance of spontaneous depassivation-repassivation transients related to metastable pitting at short immersion times could not be observed in Fig. 7d: no isolated characteristic transients can be identified because the fluctuations result from the sum of numerous corrosion processes developing simultaneously on the rather large surface area of the metal.

4.3. ENM records and EIS measurements performed on 7.5 cm² electrodes – test 6

In order to go further in the interpretation of the noise impedance and its evolution with the immersion time, another test was performed with electrodes of same size (7.5 cm²) by coupling successive EN and EIS measurements. During test 6, the electrodes were coupled through the ZRA as previously but, from time to time, the electrical circuit was opened to measure the OCP and the electrochemical impedance of each electrode. After 103 hours of immersion, both electrodes presented millimeter corrosion attacks, as shown in Fig. 8, with more damages on WE1.

Figs. 9a and 9b present the current and potential PSDs as a function of the time immersion. As in test 5, the instrumentation noise had a significant influence on both potential and current records only above 1 Hz. Fig. 9c presents the noise impedance and the impedance modulus of each electrode at only three immersion times to make the figure clearer. At short immersion times (0 to 1h40), the effect of the corrosion processes was limited and both electrodes had the same impedance modulus; as expected, Z_n was equal to the impedance modulus of each electrode. At that time, the two electrodes had a similar corrosion behavior: the current time records at 30 minutes of immersion in Fig. 10a, show bidirectional current peaks, which effectively means that pitting corrosion was developing on both electrodes. This explains why the precision of the noise impedance was much lower than in Fig. 6c where the corrosion was predominant on one electrode. When the immersion time increased, the difference in the impedance moduli of the electrodes was more and more important and the noise impedance was comprised between $|Z_1|$ and $|Z_2|$, as expected [26]. The comparative time evolution of the coupled electrode potential and the impedance moduli of each electrode in Fig. 9d shows that all three quantities vary in the same way, with a progressive slow decrease that stops after 80 hours. On the other hand, the electrode with the most important corrosion damage (WE1) had higher values of impedance modulus than WE2 at the beginning of immersion and lower values after that time: $|Z_1|$ decreased much more strongly than $|Z_2|$, by a factor of 23 against a factor of 8 for $|Z_2|$ from 1h40 to 103h of immersion. This can be explained by the simultaneous influence of a stronger thinning of the protective barrier layer and the development of larger active areas on WE1.

The current time records in Fig. 10 show bidirectionnal current fluctuations during the whole test, with a predominance of downward transients when the immersion time increased, which is consistent with the fact that WE1 suffered more corrosion damage. Even at very long immersion time (Fig. 10c), the correlation between the potential and current transients is not perfect because of

the still present influence of the corrosion processes on WE2, which explains the poor precision of the noise impedance that stands between $|Z_1|$ et $|Z_2|$.

As in the previous test, the analysis of the potential and current transients is not much informative because of the important size of the electrode surface areas exposed to solution. The WEs underwent numerous corrosion attacks (pits, crevices, corrosion product detachments…), so that the depassivation-repassivation transients superimposed and were difficult to identify. Jiang *et al.* have already noted the influence of the electrode area on the appearance of metastable pitting transients, which are better observed in the EN time records when using small electrodes [27]. Using electrodes of 0.5 cm² surface area in carbonated concrete pore solution containing chloride ions, Dong *et al.* could investigate the pitting corrosion of carbon steel from the numerous and well identified potential and current transients appearing in the first 24 hours of immersion [6]. So, the next test was performed by reducing the surface area exposed to solution from 7.5 to 1.5 cm².

4.4. ENM performed on 1.5 cm² electrodes – test 7

During test 7, the two API 5L X65 electrodes of surface area 1.5 cm^2 were immersed in the solution for 81 hours and remained connected through the ZRA during the whole test. Only one electrode (WE2) presented a millimeter corrosion attack after the test, as shown in Fig. 11.

Figs. 12a and 12b present the evolution of the potential and current PSDs measured at different immersion times. It can be seen that the PSDs were strongly affected above 1 Hz by the instrumentation noise, as in the previous tests. Fig. 12c shows that the amplitude of the noise impedance varied in a non-monotonic way, decreasing or increasing, with the time of immersion. The good precision of all Z_n curves is due to the good correlation between the potential and current fluctuations, as shown in Fig. 13, which comes from the fact that the corrosion processes occurred mainly on one electrode (WE2). As explained above, in that case Z_n is equal to the impedance modulus of the non-corroding electrode [26]. So, the non-monotonic evolution of the impedance of

the non-corroding electrode can now be attributed with certainty to the evolution of the thickness of the protective barrier layer resulting from the competition between the oxidation and reduction processes. As corrosion occurred on WE2, a part of the anodic current provided by the corrosion attacks flowed to WE1, which was the seat of reduction processes that caused damage to the barrier layer and electrode impedance decrease. As a result, the WE1 impedance varied as a function of the importance of the corrosion processes on WE2 and stabilized when a stable corrosion state was reached. This is corroborated by the similar evolution of the coupled electrode potential and the noise impedance shown in Fig. 12d.

Fig. 13 presents some time records of the potential and current fluctuations measured at different immersion times. To better see the good correlation between the variations of the two quantities at all immersion times, the current values were multiplied by a factor of -1. At the beginning of the immersion, very numerous depassivation-repassivation transients due to metastable pitting corrosion, mainly on WE2, can be observed (Fig. 13a). After a few hours, localized corrosion developed and instead of pitting transients, much longer transients of higher amplitude were present, resulting from attacks of large surface area, as in Fig. 13b. However, at some immersion times, 33h (Fig. 13c) or 46h30 (not shown), continuous metastable pitting transients appeared (Fig. 13c), as already observed in the literature [6,12], in such large numbers that they could not be separated even at the highest sampling frequency (10 Hz). After 79 hours (Fig. 13d), the corrosion phenomena were so complex (pits, crevices, detachment of corrosion products…) and numerous that identifying the various phenomena is very difficult, even on small size electrodes.

It should be noticed that the two tests performed with a continuous coupling of the electrodes led to the corrosion of a single electrode while in test 6, where the circuit was opened from time to time to perform EIS measurements, corrosion occurred on both electrodes. Complementary experiments should be performed to check if such a result can be generalized.

5. Conclusion

This paper is aimed at studying the propagation of localized corrosion on API 5L X65 carbon steel electrodes in a 0.5 M $NaHCO_3$ solution containing chloride ions using electrochemical noise measurements. While the EN technique is generally used to detect the early stage of localized corrosion, long-term experiments (about 100 hours) were performed to investigate the corrosion propagation and assess the suitability of the EN technique for such study.

The main conclusions drawn from the analysis of the EN measurements, which were all validated using two sampling frequencies to check the absence of signal aliasing, are as follows:

1. The instrumentation noise had no influence on the measured signals below 1 Hz
2. While the identification of the corrosion mechanism (metastable pitting) was possible on short times of immersion from the observation of characteristic potential and current transients, this was no longer possible on long times for studying the corrosion propagation, even on small electrodes, because of the various corrosion attacks occurring simultaneously (stable and metastable pits, crevices, detachment of corrosion products…).
3. However, the amplitude of the measured noise, which increased with time, is a clear indication that the corrosion propagation continued throughout the immersion period, which was confirmed by visual and SEM observations.
4. When working with two WEs connected with a ZRA, it is not yet clear whether corrosion propagates on both WEs or only on a single one, especially when the electrical circuit is opened to perform additional measurements (EIS or others).
5. The noise impedance, Z_n, directly derived from the PSDs of the potential and current noise, brings additional information: Z_n at 0.1 Hz was shown to vary under the double influence of the thinning of the protective barrier layers and the development of large active areas on the electrodes.

6. This was corroborated by the fact that Z_n decreased and stabilized in the same time scale as the coupled potential of the WEs.

Acknowledgements

This operation was conducted with the assistance of the « Investissements d'avenir » (FIA) program of the French government, the management of which has been entrusted to Andra (French national radioactive waste management agency).

Data availability

The raw/processed data required to reproduce these findings cannot be shared at this time due to technical or time limitations.

References

[1] G. S. Frankel, Pitting corrosion of metals. A review of critical factors, J. Electrochem. Soc. 145 (1998) 2186–2198. https://doi.org/10.1149/1.1838615.

[2] R. Newman, Pitting Corrosion of Metals, The Electrochemical Society Interface, 19 (2010) 33–37. https://doi.org/10.1149/2.F03101if.

[3] M. Saremi, E. Mahallati, A study on chloride-induced depassivation of mild steel in simulated concrete pore solution, *Cem. Concr.* 32 (2002) 1915–1921. https://doi.org/10.1016/S0008-8846(02)00895-5.

[4] M. B. Valcarce, M. Vazquez, Carbon steel passivity examined in alkaline solutions: The effect of chloride and nitrite ions, Electrochim. Acta 53 (2008) 5007–5015. https://doi.org/10.1016/j.electacta.2008.01.091.

[5] H. Nahali, L. Dhouibi, H. Idrissi, Effect of phosphate based inhibitor on the threshold chloride to initiate steel corrosion in saturated hydroxide solution, Constr. Build. Mater. 50 (2014) 87–94. https://doi.org/10.1016/j.conbuildmat.2013.08.054.

[6] Z. H. Dong, W. Shi, X. P. Guo, Initiation and repassivation of pitting corrosion of carbon steel in carbonated concrete pore solution, Corros. Sci. 53 (2011) 1322–1330. https://doi.org/10.1016/j.corsci.2010.12.028.

[7] H. Ben Mansour, L. Dhouibi, H. Idrissi, Effect of phosphate-based inhibitor on prestressing tendons corrosion in simulated concrete pore solution contaminated by chloride ions, Constr. Build. Mater. 171 (2018) 250–260. https://doi.org/10.1016/j.conbuildmat.2018.03.118.

[8] Y. M. Tang, Y. Zuo, X. H. Zhao, The metastable pitting behaviors of mild steel in bicarbonate and nitrite solutions containing Cl^-, Corros. Sci. 50 (2008) 989–994. https://doi.org/10.1016/j.corsci.2007.12.003.

[9] Y. Zhou, Y. Zuo, The inhibitive mechanisms of nitrite and molybdate anions on initiation and propagation of pitting corrosion for mild steel in chloride solution, Appl. Surf. Sci. 353 (2015) 924–932. https://doi.org/10.1016/j.apsusc.2015.07.037.

[10] K. Videm, A. M. Koren, Corrosion, passivity, and pitting of carbon steel in aqueous solutions of HCO_3^-, CO_2, and Cl^-, Corrosion, 49 (1993) 746–754. https://doi.org/10.5006/1.3316127.

[11] M. Reffass, R. Sabot, C. Savall, M. Jeannin, J. Creus, Ph. Refait, Localised corrosion of carbon steel in $NaHCO_3$/NaCl electrolytes: role of Fe(II)-containing compounds, Corros. Sci. 48 (2006) 709–726. https://doi.org/10.1016/j.corsci.2005.02.016.

[12] Y. F. Cheng, M. Wilmott, J. L. Luo, The role of chloride ions in pitting of carbon steel studied by the statistical analysis of electrochemical noise, Appl. Surf. Sci. 152 (1999) 161–168. https://doi.org/10.1016/S0169-4332(99)00328-1.

[13] M. Z. Yang, M. Wilmott, J. L. Luo, Crevice corrosion behavior of A516-70 carbon steel in solutions containing inhibitors and chloride ions, Thin Solid Films, 326 (1998) 180–188. https://doi.org/10.1016/S0040-6090(98)00517-3.

[14] Y. Hou, C. Aldrich, K. Lepkova, L. L. Machuca, B. Kinsella, Monitoring of carbon steel corrosion by use of electrochemical noise and recurrence quantification analysis, Corros. Sci. 112 (2016) 63–72. https://doi.org/10.1016/j.corsci.2016.07.009.

[15] R. A. Cottis, Interpretation of electrochemical noise data, Corrosion, 57 (2001) 265–285. https://doi.org/10.5006/1.3290350.

[16] A. M. Homborg, T. Tinga, E.P.M van Westing, X. Zhang, G.M. Ferrari, J.H.W de Wit, J.M.C. Mol, A critical appraisal of the interpretation of electrochemical noise for corrosion studies, Corrosion 70 (2014) 971–987. https://doi.org/10.5006/1277.

[17] D.A. Eden, K. Hladky, D.G. John, J.L. Dawson, EN — Simultaneous monitoring of potential and current noise signals from corroding electrodes. CORROSION'86, NACE, Houston, 1986, pp. 1–9 Paper 274.

[18] F. Huet, Electrochemical noise technique, in: P. Marcus, F. Mansfeld (Eds.), Analytical Methods in Corrosion Science and Engineering, Taylor & Francis, Boca Raton, 2005, pp. 507–570.

[19] S. Ritter, F. Huet, R. A. Cottis, Guideline for an assessment of electrochemical noise measurement devices, Mater. Corros. 63 (2012) 297–302. https://doi.org/10.1002/maco.201005839.

[20] F. Huet, K. Ngo, Electrochemical noise—Guidance for improving measurements and data analysis, Corrosion, 75 (2019) 1065–1073. https://doi.org/10.5006/3211.

[21] F. Huet, S. Ritter, Electrochemical noise measurements with dummy cells: Evaluation of a round-robin test series, Corrosion, 74 (2018) 1457–1465. https://doi.org/10.5006/3007.

[22] PSD Calculation | ECG-COMON. https://ecg-comon.org/guideline/psdcalculator/ (accessed 27 June 2021).

[23] L. Xu, H. Xiao, W. Shang, B. Wang, J. Zhu, Passivation of X65 (UNS K03014) carbon steel in NaHCO3 solution in a CO_2 environment, Corros. Sci. 109 (2016) 246–256. https://doi.org/10.1016/j.corsci.2016.04.012.

[24] U. Bertocci, C. Gabrielli, F. Huet, M. Keddam, Noise resistance applied to corrosion measurements: I. Theoretical analysis, J. Electrochem. Soc. 144 (1997) 31–37. https://doi.org/10.1149/1.1837361.

[25] U. Bertocci, F. Huet, Noise resistance applied to corrosion measurements: III. Influence of the instrumental noise on the measurements, J. Electrochem. Soc. 144 (1997) 2786–2793. https://doi.org/10.1149/1.1837896.

[26] A. Bautista, U. Bertocci, F. Huet, Noise resistance applied to corrosion measurements: V. Influence of electrode asymmetry, J. Electrochem. Soc. 148 (2001) B412–B418. https://doi.org/10.1149/1.1398277.

[27] X. Jiang, S. Nesic, F. Huet, B. Kinsella, B. Brown, D. Young, Selection of electrode area for electrochemical noise measurements to monitor localized CO_2 corrosion, J. Electrochem. Soc. 159 (2012) C283–C288. https://doi.org/10.1149/2.007207jes.

LIST OF CAPTIONS

Table 1.

Composition of the tested API 5L X65 grade carbon steel

Fig. 1. Geometry and dimensions of samples of surface area: (a) 7.5 cm² and (b) 1.5 cm².

Fig. 2. PSDs of the (a) potential noise and (b) current noise measured on dummy cells of various resistances *R* measured with I-E ranges of 6 and 60 µA.

Fig. 3. Evolution of the API 5L X65 electrode potential in 0.5 M NaHCO3 + 0.2 M NaCl (without NaCl in test 1): (a) OCP of single electrodes (S = 27.3 cm^2), (b) potential of two coupled electrodes in ZRA mode and OCP of WE1 and WE2 at some immersion times for test 6.

Fig. 4. SEM images after removal of corrosion products of (a) a micrometer pit, (b) a millimeter attack and (c) pits inside the millimeter attack on the surface of an API 5L X65 sample after 115 hours of immersion in 0.5 M $NaHCO_3$ + 0.2 M NaCl (test 3).

Fig. 5. Images of the two API 5L X65 carbon steel electrodes of surface area 7.5 cm^2 after 97 hours of immersion in 0.5 M $NaHCO_3$ + 0.2 M NaCl and corrosion products removal (test 5).

Fig. 6. PSDs of the (a) current and (b) potential fluctuations, (c) noise impedance Z_n measured at different immersion times, and (d) comparative evolution of $V_{coupled}$ and Z_n at 0.1 Hz (test 5).

Fig. 7. Time records of the potential and current fluctuations measured at different immersion times (test 5): (a) 7 h, (b) 31h30, (c) 49 h, (d) 96 h. Sampling rate: f_s = 10 Hz (a) or 1 Hz (b, c, d).

Fig. 8. Images of the two API 5L X65 carbon steel electrodes of 7.5 cm^2 surface area after 103 hours of immersion in 0.5 M $NaHCO_3$ + 0.2 M NaCl (test 6).

Fig. 9. PSDs of the (a) current and (b) potential fluctuations, (c) noise impedance Z_n with electrode impedance moduli measured at different immersion times, and (d) comparative evolution of $V_{coupled}$, $|Z_1|$, $|Z_2|$ at 0.1 Hz (test 6).

Fig. 10. Time records of the potential and current fluctuations measured at different immersion times (test 6): (a) 30 min, (b) 52h30, (c) 97h30. Sampling rate: f_s = 1 Hz.

Fig. 11. (a) Images of the API 5L X65 carbon steel electrodes of 1.5 cm^2 surface area after 81 hours of immersion in 0.5 M $NaHCO_3$ + 0.2 M NaCl, and (b) enlargement of the millimeter corrosion attack on WE2 (test 7).

Fig. 12. PSDs of the (a) current and (b) potential fluctuations, and (c) noise impedance Z_n measured at different immersion times, and (d) comparative evolution of $V_{coupled}$ and Z_n at 0.1 Hz (test 7).

Fig. 13. Time records of the potential and current fluctuations measured at different immersion times (test 7): (a) 30 min, (b) 25 h 30, (c) 33 h, (d) 79 h 30. Sampling rate: f_s = 1 Hz (a, b, d) or 10 Hz (c).

Table 1.

Composition of the tested API 5L X65 grade carbon steel.

Element	C	Mn	Si	P	S	Cu	Cr	Ni	Mo
wt%	0.031	1.38	0.285	0.008	0.001	0.193	0.034	0.399	0.023

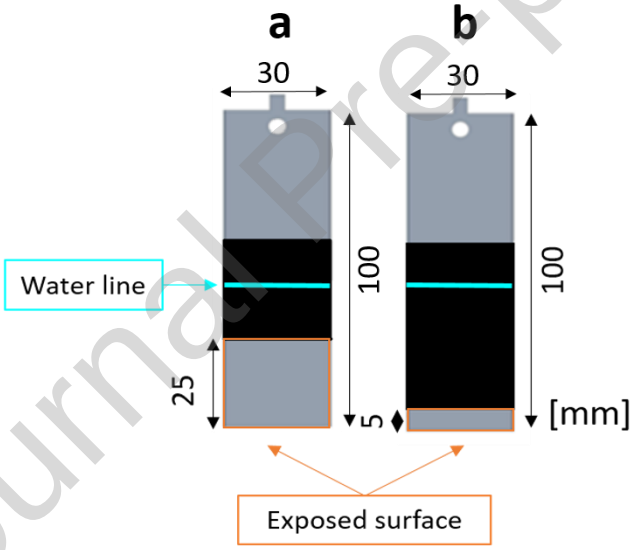

Fig. 1. Geometry and dimensions of samples of surface area: (a) 7.5 cm² and (b) 1.5 cm².

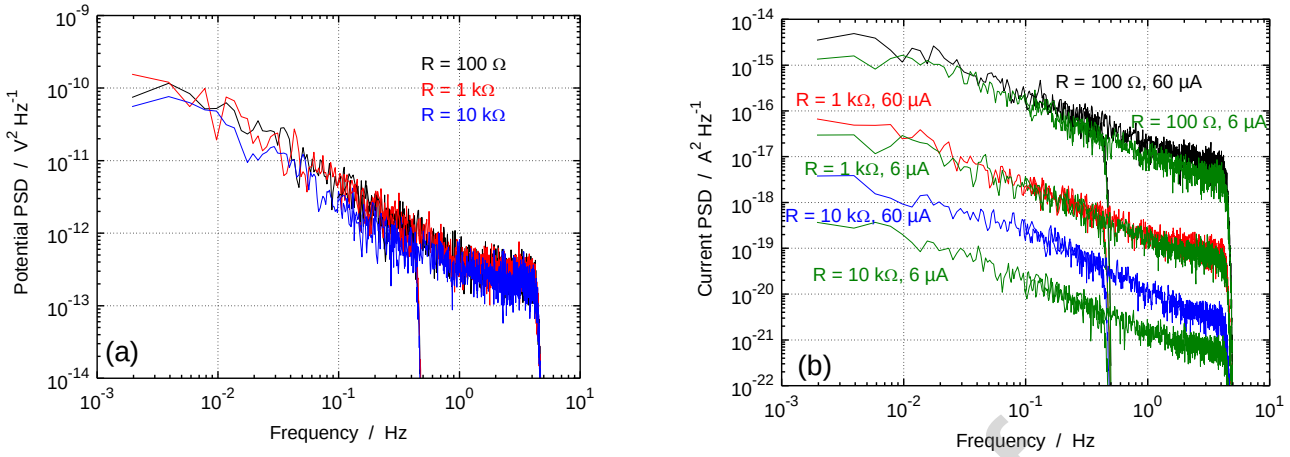

Fig. 2. PSDs of the (a) potential noise and (b) current noise measured on dummy cells of various resistances *R* measured with I-E ranges of 6 and 60 µA.

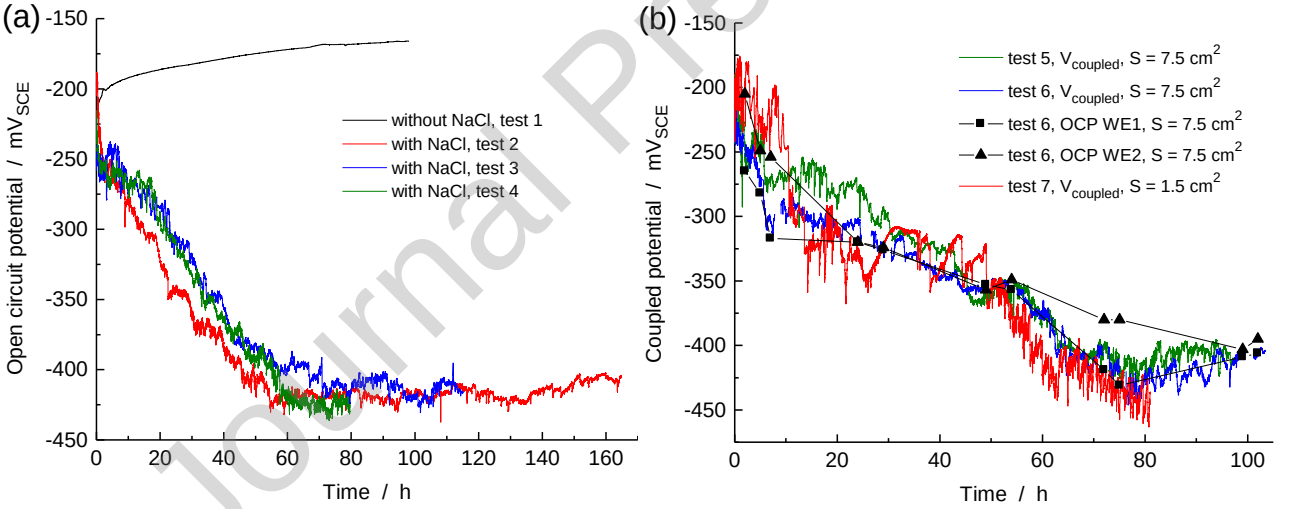

Fig. 3. Evolution of the API 5L X65 electrode potential in 0.5 M NaHCO3 + 0.2 M NaCl (without NaCl in test 1): (a) OCP of single electrodes (S = 27.3 cm^2), (b) potential of two coupled electrodes in ZRA mode and OCP of WE1 and WE2 at some immersion times for test 6.

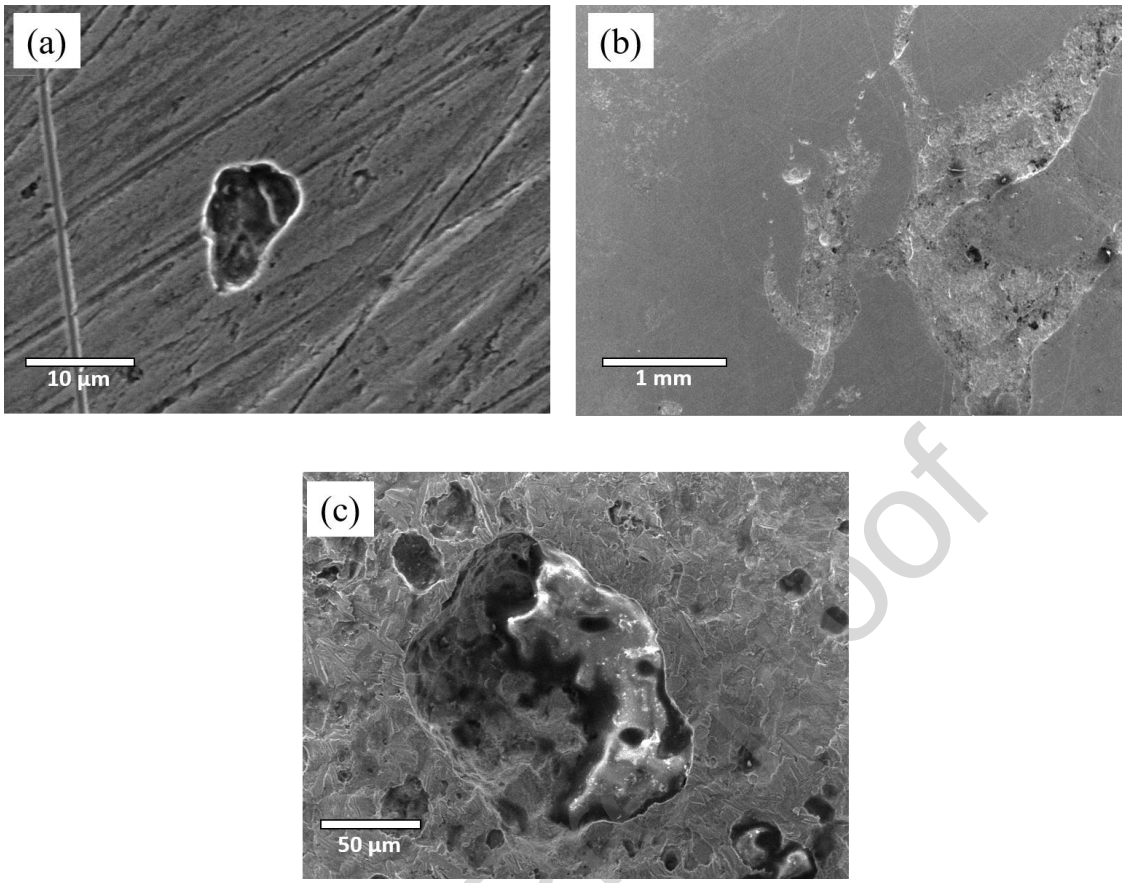

Fig. 4. SEM images after removal of corrosion products of (a) a micrometer pit, (b) a millimeter attack and (c) pits inside the millimeter attack on the surface of an API 5L X65 sample after 115 hours of immersion in 0.5 M $NaHCO_3$ + 0.2 M NaCl (test 3).

Fig. 5. Images of the two API 5L X65 carbon steel electrodes of surface area 7.5 cm^2 after 97 hours of immersion in 0.5 M $NaHCO_3$ + 0.2 M NaCl and corrosion products removal (test 5).

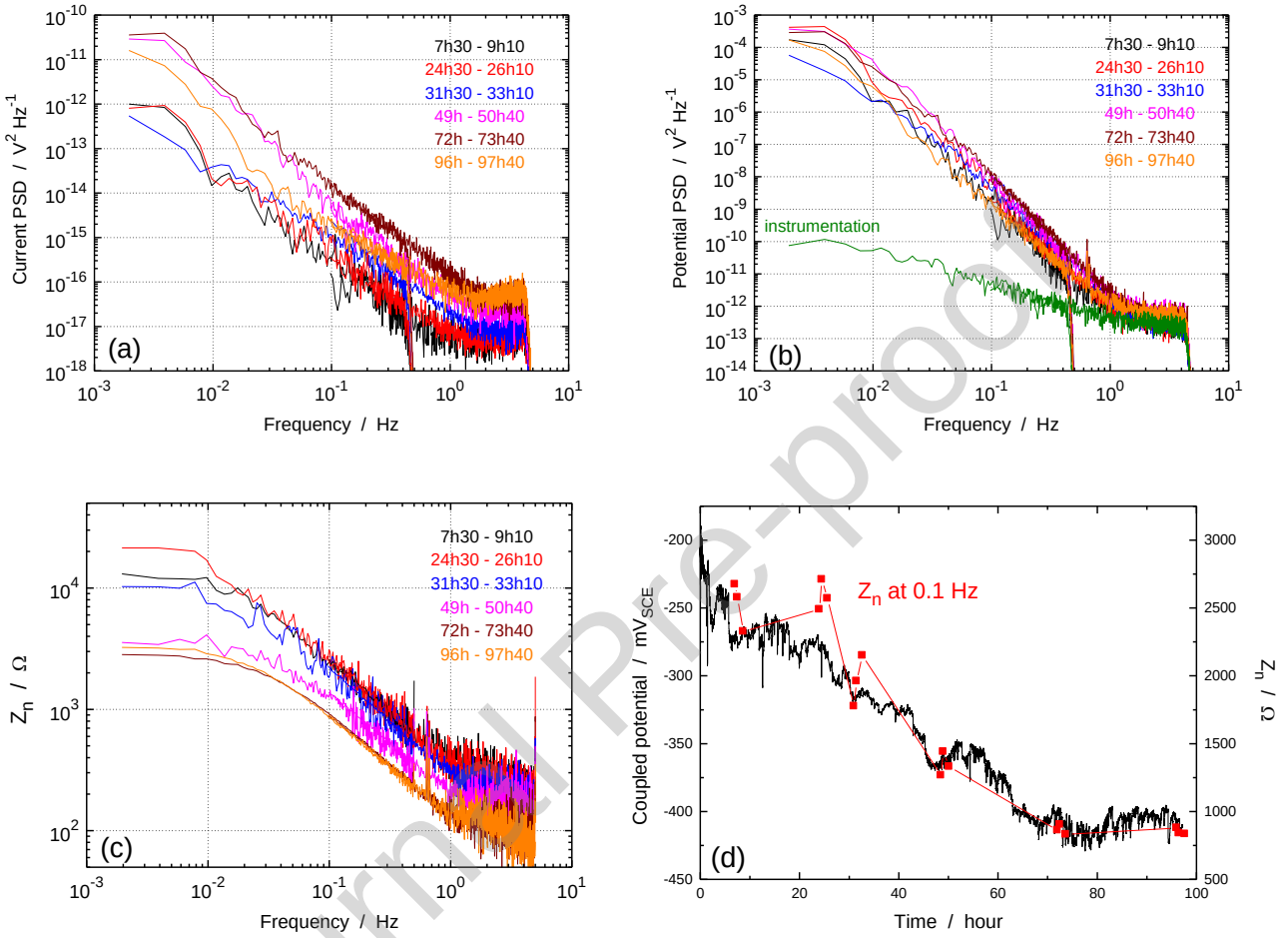

Fig. 6. PSDs of the (a) current and (b) potential fluctuations, (c) noise impedance Z_n measured at different immersion times, and (d) comparative evolution of $V_{coupled}$ and Z_n at 0.1 Hz (test 5).

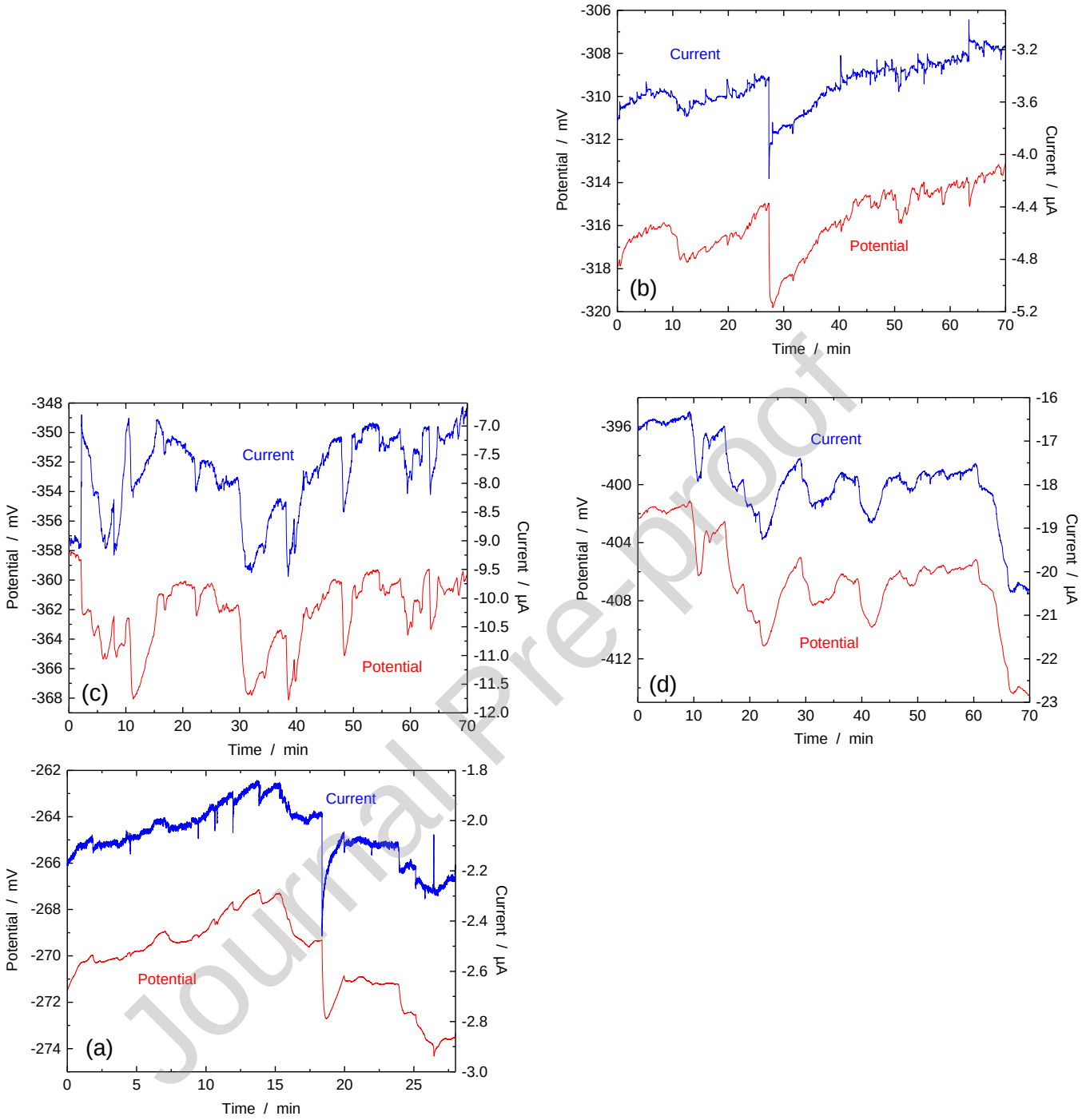

Fig. 7. Time records of the potential and current fluctuations measured at different immersion times (test 5): (a) 7 h, (b) 31h30, (c) 49 h, (d) 96 h. Sampling rate: f_s = 10 Hz (a) or 1 Hz (b, c, d).

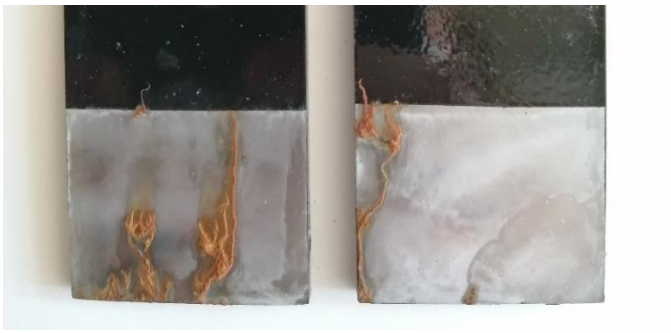

Fig. 8. Images of the two API 5L X65 carbon steel electrodes of 7.5 cm^2 surface area after 103 hours of immersion in 0.5 M $NaHCO_3$ + 0.2 M NaCl (test 6).

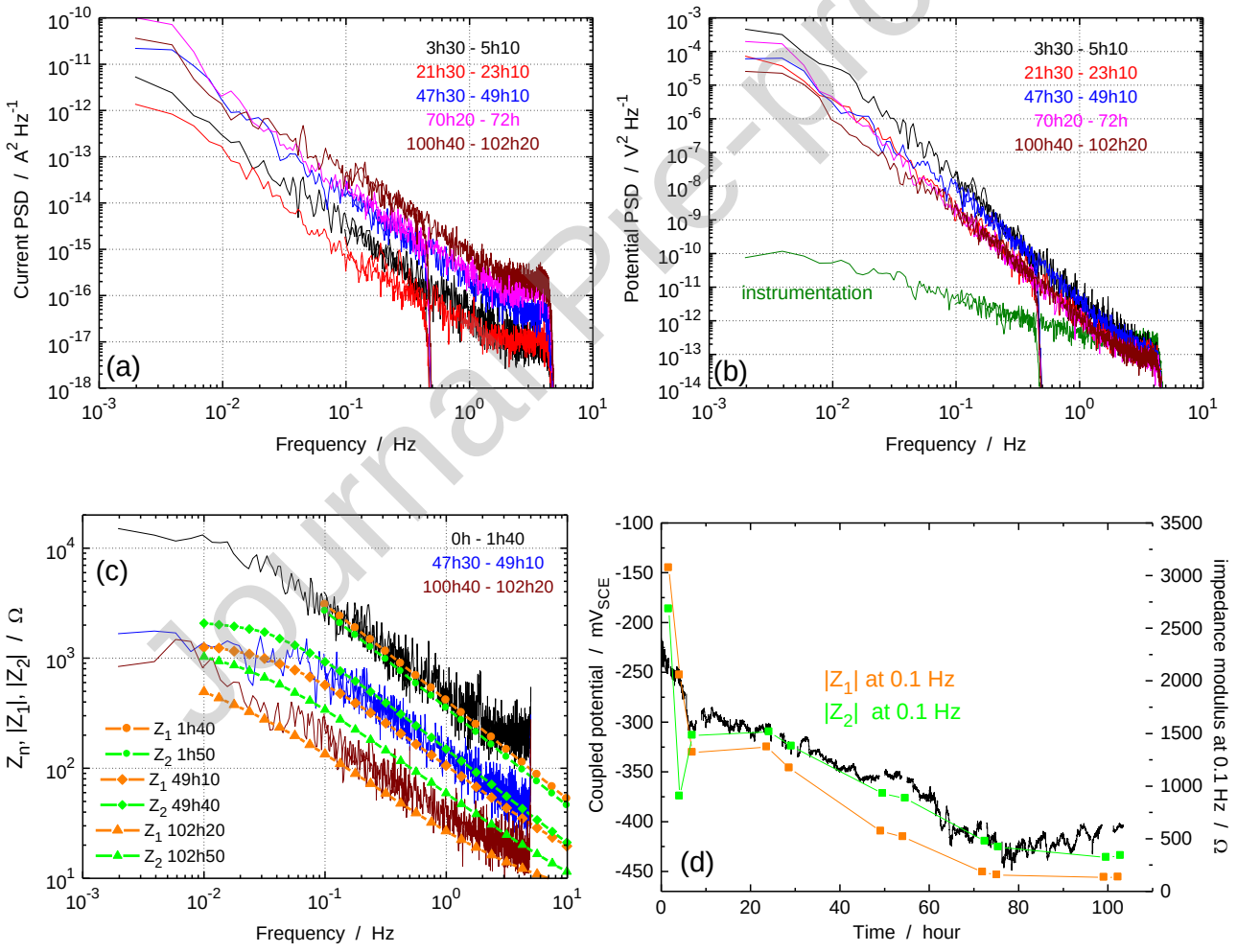

Fig. 9. PSDs of the (a) current and (b) potential fluctuations, (c) noise impedance Z_n with electrode impedance moduli measured at different immersion times, and (d) comparative evolution of $V_{coupled}$, $|Z_1|$, $|Z_2|$ at 0.1 Hz (test 6).

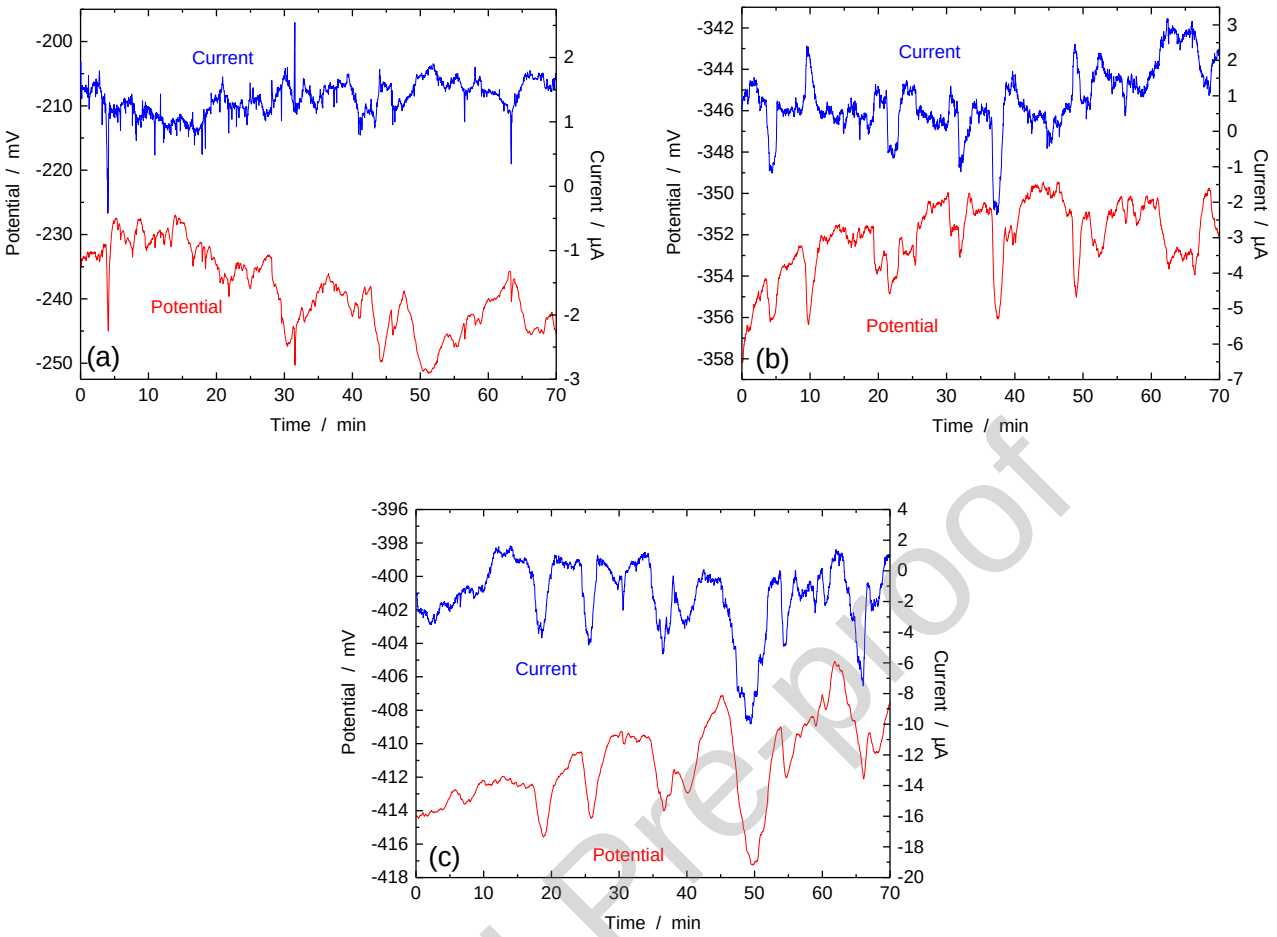

Fig. 10. Time records of the potential and current fluctuations measured at different immersion times (test 6): (a) 30 min, (b) 52h30, (c) 97h30. Sampling rate: f_s = 1 Hz.

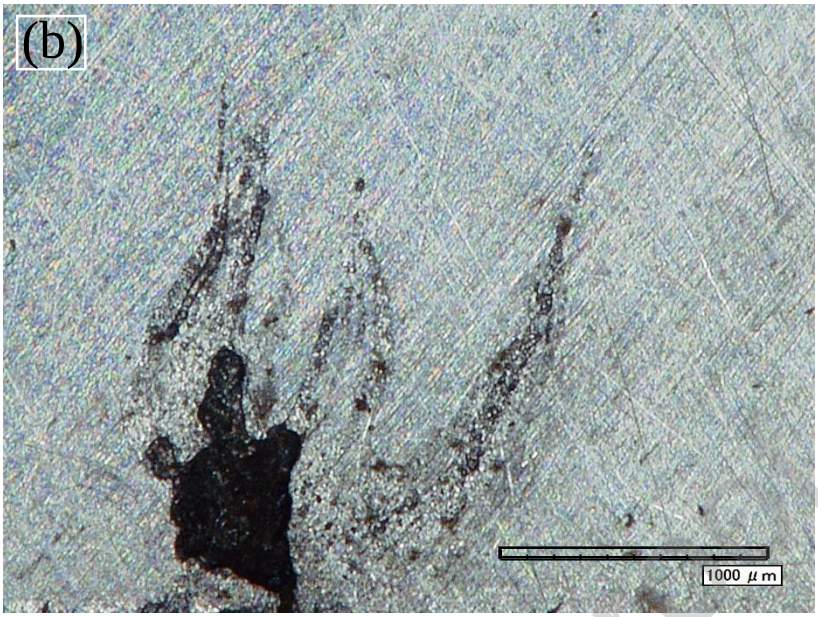

Fig. 11. (a) Images of the API 5L X65 carbon steel electrodes of 1.5 cm^2 surface area after 81 hours of immersion in 0.5 M $NaHCO_3$ + 0.2 M NaCl, and (b) enlargement of the millimeter corrosion attack on WE2 (test 7).

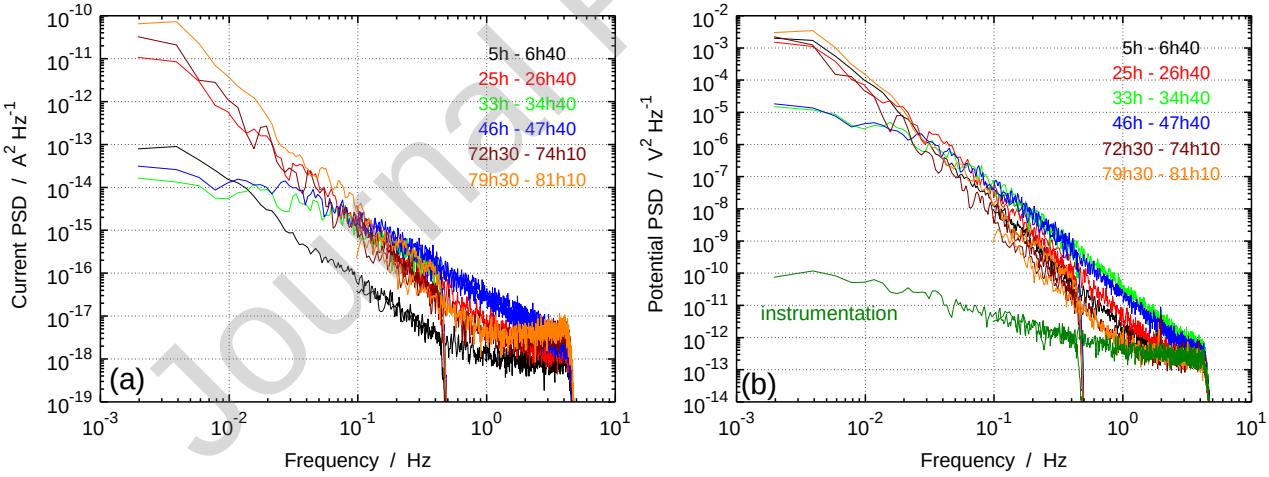

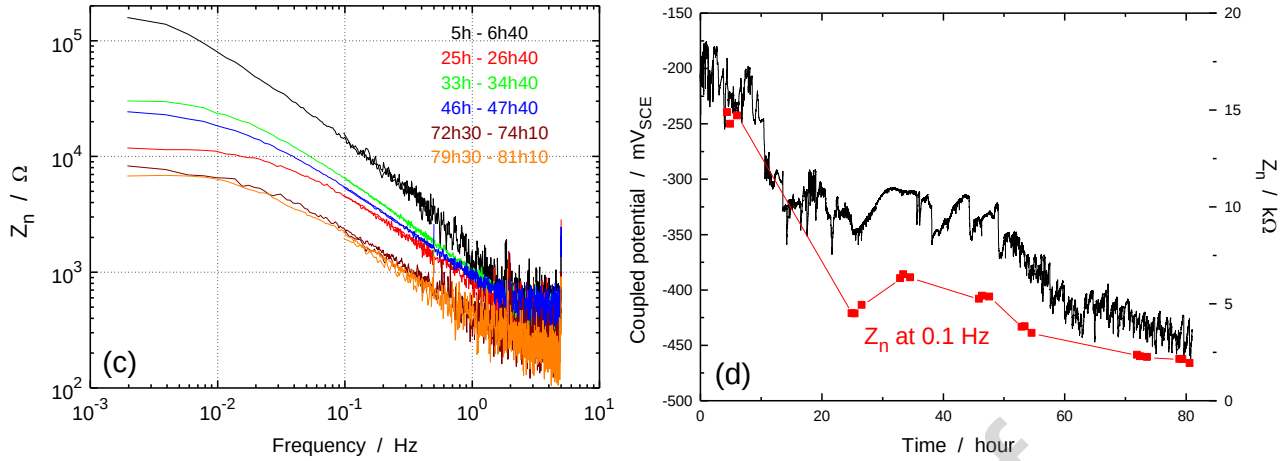

Fig. 12. PSDs of the (a) current and (b) potential fluctuations, and (c) noise impedance Z_n measured at different immersion times, and (d) comparative evolution of $V_{coupled}$ and Z_n at 0.1 Hz (test 7).

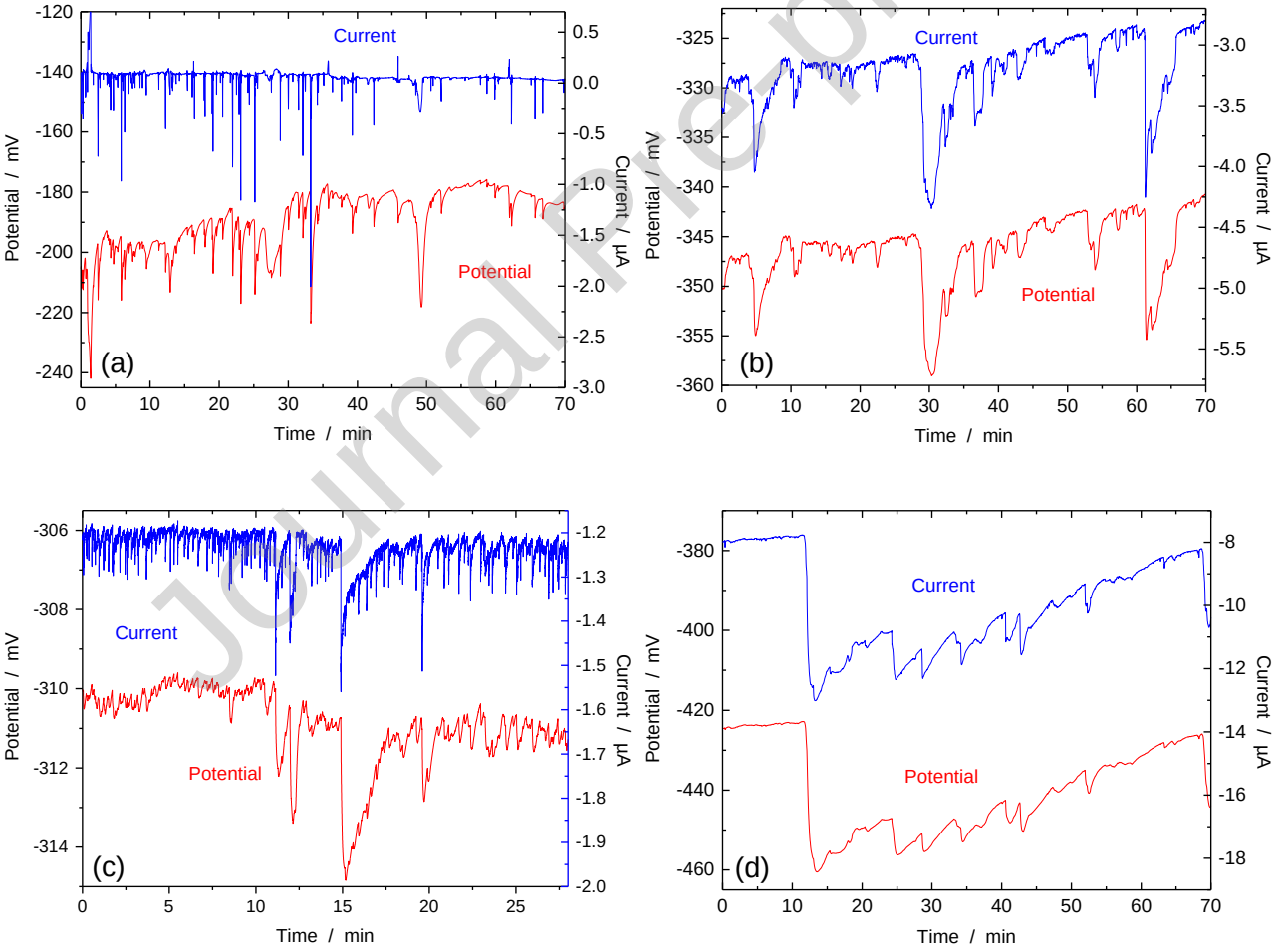

Fig. 13. Time records of the potential and current fluctuations measured at different immersion times (test 7): (a) 30 min, (b) 25 h 30, (c) 33 h, (d) 79 h 30. Sampling rate: f_s = 1 Hz (a, b, d) or 10 Hz (c).

CRedit author statement

C. Comas: Conceptualization, Methodology, Investigation, Validation, Formal analysis, Writing - Original draft, **F. Huet:** Conceptualization, Methodology, Supervision, Validation, Formal analysis, Data curation, Writing - Original draft, Visualization, Software, **K. Ngo**: Conceptualization, Methodology, Writing – Review & Editing, **M. Fregonese:** Project administration, Funding acquisition, Conceptualization, Supervision, Resources, Writing – Review & Editing, **H. Idrissi:** Supervision, Resources, Writing – Review & Editing, **B. Normand:** Supervision, Resources, writing – Review & Editing

Declaration of interests

☒ The authors declare that they have no known competing financial interests or personal relationships that could have appeared to influence the work reported in this paper.

☐The authors declare the following financial interests/personal relationships which may be considered as potential competing interests:

HIGHLIGHTS

- Study of localized corrosion of API 5L X65 carbon in $NaHCO_3$ solution with Cl^- ions
- Corrosion propagation studied with EN during long immersion times (100 h) in ZRA mode
- Corrosion mechanism identification by noise transients only at short immersion times
- Corrosion propagation may be monitored from the increase in noise amplitude
- Noise impedance follows same time evolution as the coupled potential of the WEs